Quaternary Science Reviews 77 (2013) 101–112

Contents lists available at SciVerse ScienceDirect

Quaternary Science Reviews

journal homepage: www.elsevier.com/locate/quascirev

# A Last Glacial Maximum through middle Holocene stalagmite record of coastal Western Australia climate

Rhawn F. Denniston [a,*], Yemane Asmerom [b], Matthew Lachniet [c], Victor J. Polyak [b], Pandora Hope [d], Ni An [a], Kristyn Rodzinyak [a,1], William F. Humphreys [e,f,g]

[a] Department of Geology, Cornell College, Mount Vernon, IA 52314, USA
[b] Department of Earth and Planetary Sciences, University of New Mexico, Albuquerque, NM, USA
[c] Department of Geoscience, University of Nevada-Las Vegas, Las Vegas, NV, USA
[d] Centre for Australian Weather and Climate Research, Bureau of Meteorology, Melbourne, Australia
[e] School of Animal Biology, University of Western Australia, Perth, Australia
[f] Western Australian Museum, Welshpool DC, Australia
[g] University of Adelaide, Adelaide, Australia

ARTICLE INFO

*Article history:*
Received 9 March 2013
Received in revised form
30 June 2013
Accepted 2 July 2013
Available online

*Keywords:*
Stalagmite
Oxygen
Carbon
Isotope
Indo-Australian summer monsoon
Southern westerlies
Cape Range
Australia

ABSTRACT

Stable isotope profiles of $^{230}$Th-dated stalagmites from cave C126, Cape Range Peninsula, Western Australia, provide the first high-resolution, continental paleoclimate record spanning the Last Glacial Maximum, deglaciation, and early to middle Holocene from the Indian Ocean sector of Australia. Today, rainfall at Cape Range is sparse, highly variable, and is divided more or less equally between winter and summer rains, with winter precipitation linked to northwest cloud bands and cold fronts derived from the southern mid- to high-latitudes, and summer precipitation due primarily to tropical cyclone activity. Influences of the Indo-Australian summer monsoon at Cape Range are minimal as this region lies south of the modern monsoon margin. The interaction of these atmospheric systems helps shape the environment at Cape Range, and thus C126 stalagmite-based paleoclimatic reconstructions should reflect variability in moisture source driven by changing ocean and atmospheric conditions.

The C126 record reveals slow stalagmite growth and isotopically heavy oxygen isotope values during the Last Glacial Maximum, followed by increased growth rates and decreased oxygen isotopic ratios at 19 ka, reaching a $\delta^{18}$O minimum from 17.5 to 16.0 ka, coincident with Heinrich Stadial 1. The origin of this oxygen isotopic shift may reflect enhanced moisture and lower oxygen isotopic ratios due to amount effect-driven changes in rainfall $\delta^{18}$O values from an increase in rainfall derived from tropical cyclones or changes in northwest cloud band activity, although the controls on both systems are poorly constrained for this time period. Alternatively, lower C126 stalagmite $\delta^{18}$O values may have been driven by more frequent or more intense frontal systems associated with southerly-derived moisture sources, possibly in relation to meridional shifts in positioning of the southern westerlies which have been linked to southern Australia megalake highstands at this time. Finally, we also consider the possibility of contributions of tropical moisture derived from the Indo-Australian summer monsoon. The Intertropical Convergence Zone and associated monsoon trough shifted southward during Heinrich events and other periods of high northern latitude cooling, and although clearly weakened during glacial periods, rainfall with low $\delta^{18}$O values associated with the monsoon today suggests that even small contributions from this moisture source could have accounted for some of the observed oxygen isotopic decrease. Despite a pronounced isotopic excursion coincident with Heinrich Stadial 1, no identifiable anomaly is associated with Heinrich Stadial 2.

The Holocene is also characterized by overall low $\delta^{18}$O values and rapid growth rates, with decreasing oxygen isotopic values during the earliest Holocene and at ~6.5 ka, roughly coincident with southern Australia megalake highstands. The origins of these stalagmite oxygen isotopic shifts do not appear to reflect increases in mean annual temperature but are tied here largely to changes in the $\delta^{18}$O values of precipitation and may reflect a more southerly influence of the Indo-Australian summer monsoon at this time.

C126 stalagmite carbon isotopic ratios offer an important complement to the oxygen isotopic time series. Stalagmite $\delta^{13}$C values averaged −5‰ during the Last Glacial Maximum and early deglaciation,

* Corresponding author. Tel.: +1 319 895 4306.
*E-mail address:* rdenniston@cornellcollege.edu (R.F. Denniston).
[1] Current address: Department of Earth and Planetary Sciences, McGill University, Montreal, Quebec, Canada.

0277-3791/$ – see front matter 
http://dx.doi.org/10.1016/j.quascirev.2013.07.002

and reached a plateau during the oxygen isotopic minimum at 17.5 ka. However, $\delta^{13}C$ values decreased sharply to −12‰ between 11 and 8 ka, a shift interpreted to reflect increases in plant density in response to the onset of interglacial conditions. Stalagmite $\delta^{13}C$ values at 6 ka are lower than expected for the modern $C_4$-dominated vegetation and thin soils of Cape Range, suggesting that a more $C_3$-rich environment was present during elevated rainfall conditions of the early and middle Holocene. The Cape Range stalagmite time series thus reveals for the first time the millennial-scale sensitivity of the moisture source variations in northwestern Australia, a result that has implications for precipitation dynamics across much of the continent.



## 1. Introduction

Identifying the timing and nature of regional responses to climatic change is necessary for developing a holistic view of the global climate system. This is particularly true for the Last Glacial Maximum (LGM) through the Holocene, an interval of profound environmental change, but attempts to construct an integrated picture of this period are hampered in some regions by a scarcity of the requisite high-resolution paleoenvironmental records. Western Australia is one such area that lacks high-resolution, Late Quaternary paleoclimate time series, particularly north of 30°S latitude. To date, the most continuous paleoclimate reconstructions from this region are based on terrestrial pollen and spores obtained from marine cores located off the Cape Range Peninsula (Fig. 1), but interpreting these data is complicated by limited temporal resolution, the potential for bioturbation and unconformities, and the likelihood that the pollen was sourced from a wide latitudinal transect (van der Kaars and De Deckker, 2002, 2003; van der Kaars et al., 2006). Cape Range is an area of particular interest because part of it and the adjacent Ningaloo Reef are UNESCO world heritage sites, and Cape Range and the surrounding region have a rich archeological record.

Today, Cape Range lies at the northern margin of the zone of winter precipitation associated with the southern hemisphere westerlies, and the southern margin of the interval of Western Australia experiencing the highest historical tropical cyclone activity (bom.gov.au). Cape Range also receives a considerable percentage of its winter moisture totals from northwest cloud bands, broad atmospheric systems stretching northwest–southeast and that can span much of the Australian continent (Telcik, 2003; Indian Ocean Climate Initiative, 2012). Cape Range also lies south of the margin of the Indo-Australian summer monsoon (IASM), but given the dynamic nature of the IASM during the last deglaciation (Muller et al., 2012; Denniston et al., 2013), it is conceivable that this system, too, may have once contributed significant quantities of rainfall to Cape Range (Fig. 1). Variations in the IASM, the southern hemisphere westerlies, and tropical cyclones have each been linked to extra-regional forcing, and thus globally expressed climate changes may be reflected in the interactions of these and related systems.

Despite this region's paucity of traditional paleoclimate archives, Cape Range Peninsula contains numerous caves and thus holds the potential for speleothem-based paleoenvironmental reconstruction. Here we present an absolute-dated stalagmite isotopic time series from cave C126 in Cape Range that marks the first high-resolution continental paleoclimate record from this region of Western Australia spanning the LGM, deglaciation, and early/middle Holocene. Dating by $^{230}Th$ methods reveals stalagmite growth from 26 to 15 and 11 to 6 ka, and stalagmite carbon and oxygen isotopic ratios track paleoenvironmental changes, thereby allowing a rare and detailed examination of these mechanisms by which climate variability was expressed in Western Australia during this time.

## 2. Geologic and environmental settings

### 2.1. Cape Range and Cave C126 geology

Cape Range, Western Australia lies within the Exmouth subbasin of the Carnarvon geological province, and is composed of anticlinal, middle Cenozoic marine carbonate sequences (Russell, 2004). The range itself reaches 330 m in elevation and is dissected by gorges that cut karstic limestone bedrock stretching to a coastal plain that ends in a series of raised, wave-cut terraces. Cape Range marks the closest point in Australia to the continental slope and thus remained proximal to the ocean throughout the LGM. Approximately 800 caves are identified in this area, and two stalagmites were collected in August of 1991 AD from cave C126 (22.1°S, 113.9°E), a solution pipe with lateral development at depth (approx. 54 m below the land surface; cave floor elevation approx. 50 m), that represents a typical cave morphology for this region (Hamilton-Smith et al., 1998) (Fig. 2). When visited, the cave was 21 °C with 96% relative humidity (D. Brooks, Pers. Comm.).

### 2.2. Regional climate

At Cape Range, regional climate is characterized by a mean annual temperature of 25 °C and summer temperatures as high as 47 °C (Fig. 3). Mean annual rainfall, which is episodic and often torrential, is only 280 mm, and potential evaporation rates are high (pan evaporation $\leq$ 3200 mm/year). Groundwater recharge into the unconfined aquifer system at Cape Range accounts for only 10% of average annual rainfall (Forth, 1973). Rainfall is primarily derived in roughly equal proportion from winter and summer, with the former associated with northwest cloud bands (NWCB) and fronts that are sourced at the southern mid- to high-latitudes (WAPC, 1996; Frederiksen et al., 2011). The NWCB season is from April to October, and these events represent a significant source of moisture to Western Australia, providing up to 80% of annual rainfall for northwestern Australia, particularly for (near)coastal sites (Wright, 1997; Telcik, 2003). NWCB can reach thousands of km in length, stretching from the Intertropical Convergence Zone (ITCZ) on the northwest to a cold front at their southeastern end. The development of NWCB is influenced by regional ocean and atmosphere variations including strong winds and high sea surface temperatures (SST) (Meehl, 1993), and particularly SST anomalies in the eastern Indian Ocean (Telcik, 2003). These ocean temperatures are, in turn, influenced by a number of factors including the El Niño-Southern Oscillation (ENSO) and the Indian Ocean Dipole (IOD) (Telcik, 2003). NWCB are also strongly correlated with the latitude of the subtropical ridge along eastern Australia, and in wet years, are associated with an equatorward shift of the subtropical ridge and associated frontal systems tied to the mid-latitude westerlies (Pittock, 1975). Pronounced variability in NWCB has been documented over the last fifty years, with NWCB modes having increased by approximately 25% or more for each of the 1975–1994 AD and 1997–2006 AD periods, compared with the 1949–1968 AD

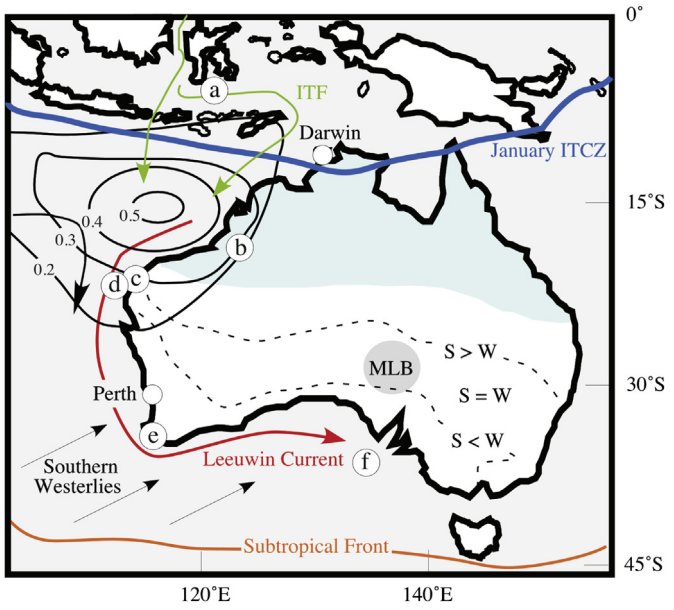


**Fig. 1.** Map of Australia with locations of sites discussed in text. a. Flores Sea core VM33-80 (Muller et al., 2012); b. Fitzroy River and Lake Gregory (Wyrwoll and Miller, 2001) and Ball Gown Cave (Denniston et al., 2013); c. Cape Range and C126 (this study); d. FR1095/9C17 marine core (van der Kaars and De Deckker, 2002); e. Cape Leeuwin (Treble et al., 2005); f. MD03-2611 marine core (De Deckker et al., 2012). Dotted and dashed lines represent zones of precipitation seasonality (S = summer, W = winter) (Gentilli, 1986). MLB = megalake basins discussed in text; contours define average annual tropical cyclone occurrence (bom.gov.au). Blue shaded area represents region of IASM. ITF = Indonesian Throughflow.

period (Indian Ocean Climate Initiative, 2012). Summer rains are tied largely to tropical cyclones and are capable of delivering large amounts of rainfall during some austral summers, with such events occurring an average of once per 3–5 years (bom.gov.au; Milton, 1980; Dare et al., 2012), and occasionally deeply flooding some caves (Humphreys, 1991a,b). Tropical cyclone activity is tied, in part, to SST, most notably through ENSO (Nicholls, 1992; Dare and McBride, 2011), and in Western Australia is highest just north of Cape Range and decreases sharply with distance south (Fig. 1).

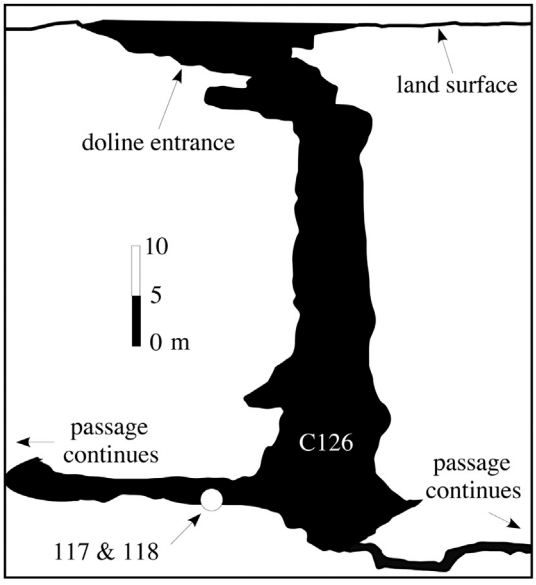


**Fig. 2.** Map of Cave C126. Redrawn from Humphreys (1991a,b: Appendix C: 11–12). Cave surveyed by D. Brooks, M. East, A. Humphreys, J. Bass and R. Wood, original drawing by R. Wood.

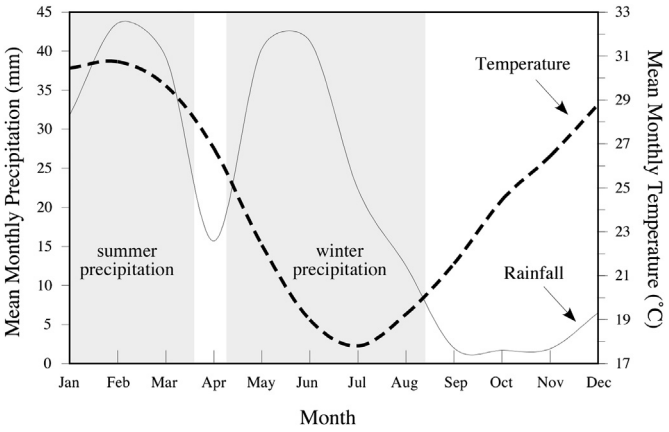


**Fig. 3.** Climatological data for Cape Range (bom.gov.au).

The Leeuwin Current, an anomalous poleward-flowing eastern boundary current, develops off-shore of Cape Range and transports warm water southward along the Western Australian margin and eastward along the South Australian margin, reaching as far as Tasmania in some years (Fig. 1). The Leeuwin Current has been tied to temperature and rainfall patterns in southwestern Australia (Pearce and Pattiaratchi, 1999), and impacts sea breezes at Cape Range but the direct impacts of the Leeuwin Current on the climate of northwestern Australia, including Cape Range, remain poorly understood.

Regional vegetation is dominated by plants utilizing the $C_4$ photosynthetic pathway, with $C_4$ representing more than 90% by subdivisional percent, and 66% of the total plant species. Plant types are largely tussock grass (*Triodia*), with lesser amounts of *Acacia*, *Eucalyptus*, and *Banksia* (Hattersley, 1983). *Ficus* is commonly associated with cave entrances and roots can penetrate to great depth in sinkholes and fissures, however *Triodia* completely dominates the high country in the area of C126. Overall, plant density is sparse, and soils are thin and weakly developed on the uplands that overlie the caves.

## 3. Methods

### 3.1. U/Th dating

Two broken and down cylindrical stalagmites, C126-117 and C126-118, were collected in 1991 AD from the floor of the main chamber of C126. Both samples are composed of clear, dense, and finely crystalline calcite, interlayered in many areas with sub-mm-scale clay laminae (Fig. 4). Parallel cuts were used to slab the stalagmites in line with the vertical growth axis, and chronologies were established by using a computer-guided drill to mill approximately 100–200 mg from the central growth axis of the slabs for $^{230}$Th dating at the University of New Mexico Radiogenic Isotope Laboratory. Calcite powders were dissolved and spiked with a mixed $^{229}$Th–$^{233}$U–$^{236}$U tracer, and the sample and spike were homogenized by drying the solution on a hot plate and then redissolved in 7N $HNO_3$. To ensure that any organic material included within the calcite was destroyed, the solution was heated in a mixture of 14N $HNO_3$ and perchloric acid. Next, U and Th fractions were isolated using standard column chemistry methods (Chen et al., 1986).

Isotopic ratios were measured using either a Micromass Sector 54 thermal ionization mass spectrometer (TIMS) or a Thermo Neptune multi-collector inductively coupled plasma mass spectrometer (MC-ICP-MS) (Table 1). For analysis on the TIMS, all

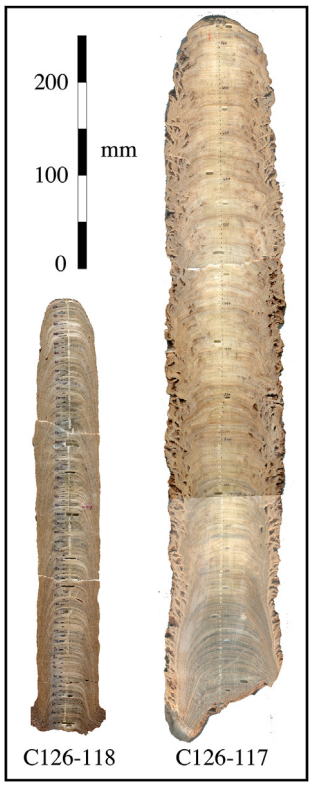


**Fig. 4.** Photographs of stalagmites C126-117 and C126-118. Note interlayered mud laminae at base of C126-117.

isotopes of interest ($^{236}U$, $^{235}U$, $^{234}U$, $^{233}U$, $^{232}Th$, $^{230}Th$, $^{229}Th$) were measured using a high-abundance sensitivity filter on an ion-counting Daly multiplier, requiring very little background correction even for samples with large $^{232}Th$. Multiplier dark noise was about 0.3 counts per second. A NBL-112A U standard was measured during the course of this study and was always in the range of 0.1% of the accepted $^{234}U/^{238}U$ ratio. For analysis on the MC-ICP-MS, the U and Th fractions were dissolved in 4 ml of a 3% $HNO_3$ solution which was then aspirated into the instrument using a Cetac Aridus II low flow (50–100 μl/min) desolvating nebulizer system. U and Th separates were run as static routines where all isotopes were measured in Faraday cups, with the exception of $^{234}U$ and $^{230}Th$ which were measured using the secondary electron multiplier (SEM). Gains between the SEM and the Faraday cups were determined using standard solutions of NBL-112 for U and an in-house $^{230}Th$–$^{229}Th$ standard for Th that were typically measured after every fifth sample. U and Th blanks were less than 20 pg, and corrections for unsupported $^{230}Th$ were made using an initial $^{230}Th/^{232}Th$ ratio of 4.4 ppm, the mean crustal silicate value, with an uncertainty of ±100%. Decay constants used were those reported by Cheng et al. (2000).

### 3.2. Stable isotopic analysis

Stable isotopic ratios were obtained from powders drilled from the center of each slab using a 0.5 mm-diameter drill bit at average spatial (temporal) intervals of 5 mm (34 yr) and 1 mm (71 yr) for C126-117 and C126-118, respectively, and analyzed for $\delta^{13}C$ and $\delta^{18}O$ values at the Las Vegas Isotope Science Laboratory in the Department of Geosciences at the University of Nevada Las Vegas. Stable isotopic ratios were measured using phosphoric acid digestion at 70 °C with a ThermoElectron Delta V Plus mass spectrometer linked to a Kiel IV automated carbonate preparation device. Six internal carbonate standards calibrated against NBS-18 and NBS-19 were included with each run and yielded an analytical precision for both carbon and oxygen of better than 0.1‰ (1σ).

## 4. Results

### 4.1. Chronology

$^{230}Th$ dating reveals continuous growth from 26 to 15 ka for C126-118 and 11 to 6 ka for C126-117 (Table 1; Fig. 5). Intervals available for dating were limited by the high abundances of mud laminae that increased detrital Th abundances, and as a result, of the 27 dates obtained for these stalagmites, the nine with errors in excess of 10% were excluded from the growth model. One area where the chronology suffered from these limitations is the bottom (oldest) 150 mm of C126-117 where mud layers are interspersed within the stalagmite calcite at such fine scale that physical isolation of clean calcite was impossible in all but one area: 30 mm (Fig. 4). Taken at face value, the $^{230}Th$ dates can be interpreted as representing a substantial increase in growth rates after 7 ka or an interruption in growth prior to this time. However, as only one date anchors the oldest portion of the chronology, age constraints alone cannot identify growth hiatuses, and the abundant mud laminae complicate their identification by petrographic analysis. Without clear evidence for a hiatus of significant temporal duration, such as a corrosion layer, we assume continuous stalagmite growth.

### 4.2. Controls on stalagmite $\delta^{13}C$ and $\delta^{18}O$ values

The C126 paleoclimate record is based on the carbon and oxygen isotopic ratios of stalagmite calcite, the utility and limitations of which have been reviewed for a variety of settings (Mickler et al., 2004; Fairchild et al., 2006; Lachniet, 2009) and thus the following discussion represents an abbreviated overview of this topic. Stalagmite oxygen isotopic ratios reflect the oxygen isotopic composition of infiltrating fluids and the temperature dependence of isotopic fractionation associated with calcium carbonate crystallization (−0.2‰/°C) (Kim and O'Neil, 1997).

Carbon isotopic ratios in speleothem carbonate can reflect multiple influences, most of which are tied, directly or indirectly, to climate. Speleothem carbon is sourced from carbonate bedrock and carbon dioxide derived from the soil and the atmosphere. The proportion of carbon dioxide derived from atmospheric vs soil sources varies as a function of vegetation density (Hellstrom et al., 1998) and soil respiration rates (Genty et al., 2003), with atmospheric $CO_2$ playing an important role in shallow and poorly vegetated soils (Cerling, 1984; Frumkin et al., 2000). The $\delta^{13}C$ values of soil $CO_2$ itself reflect the relative abundances of $C_4$ and $C_3$ vegetation, with $C_3$ values approximately 15‰ lower than $C_4$ (−27‰ vs −12‰) (Smith and Epstein, 1971; Cerling, 1984); the average $\delta^{13}C$ value of the Last Glacial period atmosphere was considerably higher than during the early Holocene, with LGM $\delta^{13}C$ values of approx. −6‰ (Kohler et al., 2010). Isotopic enrichment of $^{13}C$ by ~10‰ occurs between soil gas and stalagmite carbonate (Hendy, 1971), and, in some cases, diffusion-induced fractionation can also increase $\delta^{13}C$ values of soil gas by ~4‰ (Cerling, 1984; Romanek et al., 1992). Assuming a closed system, bedrock carbonate $\delta^{13}C$ values of 0‰ (a common value for the Tertiary; Saltzman and Thomas, 2012), and no diffusion-related fractionation, then end-member $C_3$ ($C_4$) vegetation should yield stalagmite carbonate with $\delta^{13}C$ values of approximately −8‰ (−1‰) (Dorale et al., 1992; Denniston et al., 2007). Secondary effects such as precipitation of calcite in voids above the cave (Prior Calcite Precipitation, PCP) (Baker et al., 1997) have been shown to increase

**Table 1**
U/Th isotopic ratios and $^{230}$Th ages of C126 stalagmites.

| Stalagmite | Distance to base (mm) | $^{238}$U (ng/g) | $^{232}$Th (pg/g) | $\delta^{234}$U[a] (corr'd) | Error[b] | $^{230}$Th/$^{238}$U (activity) | Error | $^{230}$Th/$^{232}$Th (ppm) | Error | Uncorrected Age (yr) | Error (yr) | Corrected[c] Age (yr) | Error (yr) | Method | Applied to age model |
|---|---|---|---|---|---|---|---|---|---|---|---|---|---|---|---|
| 117 | 30 | 491.7 | 9480 | 806.9 | 11.2 | 0.1653 | 0.004 | 141.6 | 2.4 | 10,410 | 260 | 10,100 | 400 | TIMS | X |
| 117 | 240 | 196.0 | 4367 | 743.8 | 3.5 | 0.1120 | 0.004 | 83.0 | 2.7 | 7218 | 240 | 6850 | 440 | TIMS | X |
| 117 | 407 | 129.8 | 3239 | 753.4 | 5.7 | 0.1098 | 0.002 | 72.6 | 1.7 | 7030 | 120 | 6620 | 430 | TIMS | X |
| 117 | 520 | 108.7 | 2026 | 750.8 | 7.9 | 0.1036 | 0.006 | 91.8 | 5.2 | 6630 | 380 | 6330 | 490 | TIMS | X |
| 117 | 602 | 131.1 | 7655 | 744.3 | 14.6 | 0.1046 | 0.005 | 29.6 | 1.4 | 6720 | 330 | 5750 | 1020 | TIMS | |
| 117 | 729 | 97.0 | 2223 | 740.3 | 1.9 | 0.0948 | 0.001 | 68.2 | 1.0 | 6130 | 60 | 5750 | 390 | MC-ICP-MS | X |
| 117 | 768 | 73.0 | 2064 | 738.4 | 2.0 | 0.0985 | 0.002 | 57.6 | 1.5 | 6390 | 110 | 5920 | 490 | MC-ICP-MS | X |
| 118 | 6 | 69.9 | 15,573 | 814.7 | 13.3 | 0.3900 | 0.017 | 28.9 | 1.3 | 25,940 | 1310 | 22,420 | 3750 | TIMS | |
| 118 | 9 | 88.8 | 16,179 | 809.5 | 1.9 | 0.4026 | 0.003 | 36.5 | 0.3 | 26,970 | 210 | 24,100 | 2880 | TIMS | |
| 118 | 11 | 73.7 | 5964 | 863.2 | 3.7 | 0.3936 | 0.003 | 80.3 | 1.0 | 26,390 | 190 | 25,120 | 1290 | MC-ICP-MS | X |
| 118 | 99 | 51.6 | 21,821 | 821.2 | 3.3 | 0.3799 | 0.003 | 14.8 | 0.1 | 25,100 | 220 | 18,320 | 6790 | TIMS | |
| 118 | 110 | 47.6 | 3151 | 881.7 | 3.4 | 0.3312 | 0.003 | 82.6 | 1.4 | 21,450 | 210 | 20,420 | 1050 | MC-ICP-MS | X |
| 118 | 133 | 50.7 | 2142 | 874.0 | 16.9 | 0.3025 | 0.013 | 118.1 | 5.3 | 18,970 | 870 | 18,320 | 1080 | TIMS | X |
| 118 | 159 | 66.2 | 27,683 | 830.4 | 2.9 | 0.3485 | 0.002 | 13.8 | 0.1 | 22,700 | 170 | 16,020 | 6690 | TIMS | |
| 118 | 180 | 54.5 | 9768 | 866.9 | 7.2 | 0.3268 | 0.002 | 30.1 | 0.2 | 21,260 | 160 | 18,430 | 2830 | MC-ICP-MS | |
| 118 | 191 | 70.5 | 91,029 | 801.6 | 2.3 | 0.4147 | 0.002 | 5.3 | 0.0 | 28,010 | 180 | 5390 | 22,620 | TIMS | |
| 118 | 205 | 53.0 | 3777 | 903.1 | 3.4 | 0.3033 | 0.003 | 70.3 | 1.1 | 19,200 | 200 | 18,110 | 1110 | MC-ICP-MS | X |
| 118 | 226 | 47.6 | 3992 | 907.1 | 3.1 | 0.3098 | 0.004 | 61.0 | 1.1 | 19,610 | 260 | 18,320 | 410 | MC-ICP-MS | X |
| 118 | 241 | 50.8 | 1663 | 881.5 | 18.3 | 0.2762 | 0.013 | 139.3 | 7.4 | 17,130 | 920 | 16,630 | 1040 | TIMS | X |
| 118 | 286 | 52.4 | 5838 | 876.9 | 3.1 | 0.2873 | 0.002 | 42.6 | 0.4 | 17,910 | 150 | 16,210 | 1710 | TIMS | |
| 118 | 317 | 56.7 | 245 | 909.6 | 11.1 | 0.2865 | 0.018 | 1095.6 | 183.9 | 17,530 | 1190 | 17,460 | 1190 | TIMS | X |
| 118 | 343 | 45.5 | 1370 | 915.8 | 2.3 | 0.2778 | 0.003 | 152.5 | 4.7 | 17,320 | 180 | 16,860 | 490 | MC-ICP-MS | X |
| 118 | 385 | 57.5 | 4120 | 930.2 | 3.5 | 0.2887 | 0.003 | 66.5 | 1.2 | 17,910 | 210 | 16,820 | 1110 | MC-ICP-MS | X |
| 118 | 451 | 104.9 | 1780 | 919.5 | 2.1 | 0.2591 | 0.002 | 252.1 | 10.5 | 16,020 | 140 | 15,760 | 300 | MC-ICP-MS | X |
| 118 | 462 | 75.1 | 4441 | 908.7 | 3.0 | 0.2568 | 0.002 | 71.7 | 0.8 | 15,950 | 110 | 15,040 | 910 | MC-ICP-MS | X |
| 118 | 475 | 80.8 | 22,139 | 897.0 | 11.1 | 0.2889 | 0.002 | 17.4 | 0.2 | 18,170 | 160 | 13,900 | 4280 | MC-ICP-MS | |
| 118 | 481 | 92.0 | 1659 | 877.4 | 13.3 | 0.2471 | 0.009 | 226.4 | 9.3 | 15,250 | 590 | 14,970 | 650 | TIMS | X |

[a] $\delta^{234}U_{meas'd} = [(^{234}U/^{238}U)_{meas'd}/(^{234}U/^{238}U)_{eq} - 1] \times 10^3$, where $(^{234}U/^{238}U)_{eq}$ is secular equilibrium activity ratio: $\lambda_{238}/\lambda_{234} = 1.0$. Values are reported as permil.
[b] Errors are at the $2\sigma$ level.
[c] The initial $^{230}$Th/$^{232}$Th atomic ratio of $4.4 \times 10^{-6} \pm 4.4 \times 10^{-6}$ was used to correct measured $^{230}$Th/$^{232}$Th ratios.

dripwater, and thus stalagmite $\delta^{13}C$ values by up to several permil while changes in $CO_2$ out-gassing or drip rate across the stalagmite surface have also been demonstrated to alter $\delta^{13}C$ values of speleothem carbonate by kinetic effects that interfere with equilibrium exchange between various carbon species in the fluid (Mickler et al., 2004).

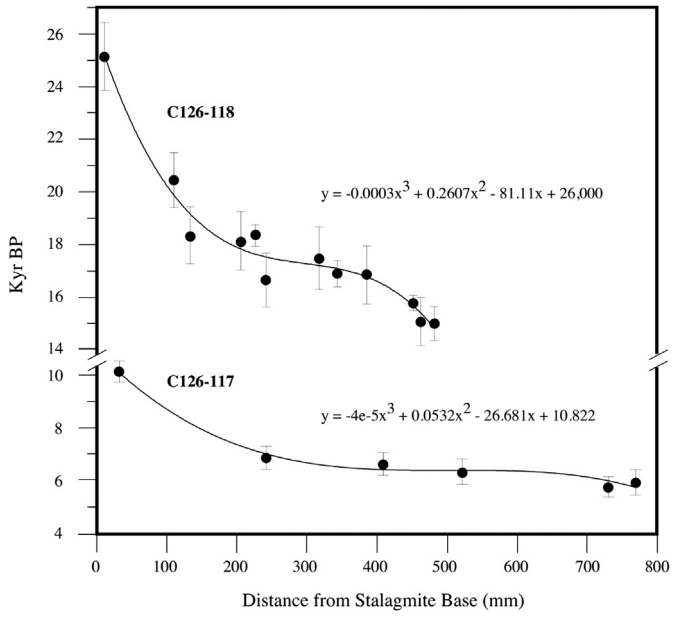


**Fig. 5.** C126 stalagmite growth models with two standard deviation errors. Equations reflect age models. Ages excluded from age models (i.e., dates with two standard deviation errors greater than ±10%) are not shown but are presented in Table 1.

The stable isotopic values of infiltrating fluids can be altered by evaporative enrichment of $^{18}O$ prior to infiltration (Denniston et al., 1999) or by processes occurring between the soil and the stalagmite surface (Mickler et al., 2006; Lachniet, 2009). Testing for these effects is best accomplished through analysis of multiple, coeval samples from the same cave because only stalagmites growing in isotopic equilibrium with unadulterated dripwaters would yield similar isotopic values and trends (Dorale and Liu, 2009). Other methods involve assessing the nature of isotopic covariance within individual growth layers (Hendy, 1971) although the reliability of these techniques has recently been called into question (Dorale and Liu, 2009; Day and Henderson, 2011).

Coeval stalagmites were not obtained from C126, however oxygen isotopic values at the top of C126-118 and bottom of C126-117 are both approx. −7.8‰, tentative evidence supporting equilibrium crystallization. Interdependence of $\delta^{13}C$ and $\delta^{18}O$ values has also been suggested as indicating disequilibrium crystallization (Mickler et al., 2004), and carbon and oxygen isotopic ratios in C126-118 display only weak covariance ($R^2 = 0.04$) while $\delta^{18}O$ and $\delta^{13}C$ values in C126-117 are more strongly covariant ($R^2 = 0.54$) (Fig. 6). These results suggest that the latter experienced some degree of non-equilibrium crystallization, or that climate and soil $CO_2$ variations changed in concert. For example, several environmental factors could similarly affect both carbon and oxygen isotopic ratios in stalagmite calcite, particularly in the tropics (e.g., wetter climates reducing PCP and therefore lowering stalagmite $\delta^{13}C$ values while simultaneously reducing pre-infiltration evaporation such that water $\delta^{18}O$ values remain low from a lack of evaporative $^{18}O$ enrichment). The high correlation between carbon and oxygen isotopic values in C126-117 does not therefore necessarily imply disequilibrium, nor does it necessarily suggest a disconnect from paleoenvironmental conditions (Lachniet, 2009) because climate could have been a common driver of both $\delta^{18}O$ and $\delta^{13}C$ values.

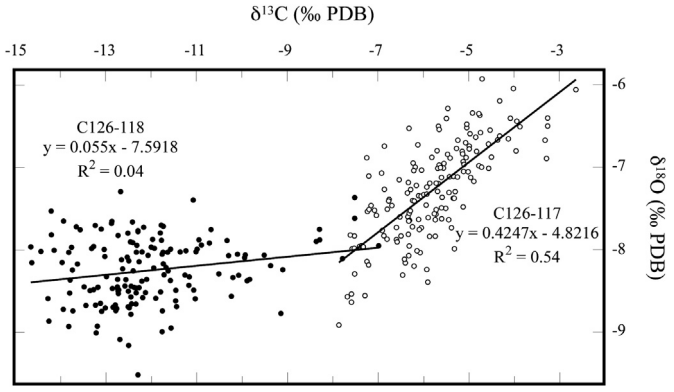


**Fig. 6.** Comparison of carbon and oxygen isotopic ratios as an indicator for isotopic equilibrium crystallization of C126 stalagmite calcite.

## 5. Discussion

### 5.1. Origins of C126 stalagmite oxygen isotopic variability

The C126 stalagmite stable isotopic time series contains significant, short-term variability (Fig. 7), but identifying the origins of isotopic dynamics at these scales is not necessarily straightforward, and thus we focus our interpretation on millennial-scale trends. The most pronounced features of the C126 oxygen isotopic record are a $\delta^{18}O$ minimum from 17.5 to 16.0 ka, a second decrease in $\delta^{18}O$ values that defines the earliest Holocene, and a smaller oxygen isotopic minimum at ~6.5 ka. Evaluating stalagmite oxygen isotopic ratios during a period of rapidly changing glacial boundary conditions involves assessing the relative influences of a number of variables including temperature and the isotopic composition of meteoric precipitation, the latter being a reflection of its source area and evolution during transport (Dansgaard, 1964). Although significant attention has been paid to the modern and paleoclimatology of the IASM-dominated regions of tropical northwestern Australia and the winter precipitation-dominated southwestern Australia, origins of rainfall variability in the Cape Range region remain far less well understood.

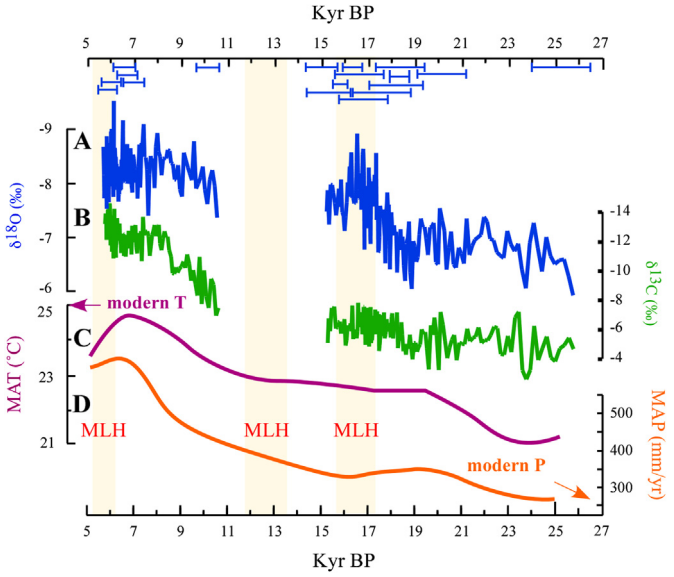


**Fig. 7.** C126 stalagmite (a) oxygen and (b) carbon isotopic time series (this study); marine core pollen transfer function-based mean annual temperature (MAT) (c) and mean annual precipitation (MAP) (d) for Cape Range region based on analysis of sediment samples from major rivers bordering the ocean in the Cape Range region (van der Kaars et al., 2006); vertical yellow bars represent periods megalake level highstands (MLH) from South Australia (Cohen et al., 2011); horizontal blue bars denote two sigma age ranges for respective $^{230}Th$ dates on C126 stalagmites.

### 5.2. Influences of temperature

Previous determinations of continental Australian deglacial paleo-temperature changes include isoleucine epimerization of radiocarbon-dated fossil emu eggshells from the Australian interior, which yielded a rapid temperature rise starting at 16 ka, with maximum warming of 9 °C between the LGM and the Holocene (Miller et al., 1997). For Cape Range, pollen transfer functions applied to assemblages obtained from a marine core suggest a 4 °C increase in mean annual temperature between the LGM and early Holocene, with rapid temperature rises from 23 to 19 and 11 to 7 ka (van der Kaars et al., 2006) (Fig. 7). Because temperatures in deep, poorly ventilated caves such as C126 typically approximate the local mean annual temperature, calcite crystallization temperatures should have tracked regional climate trends, and this parameter could in principle be estimated based on the measured stalagmite $\delta^{18}O$ values if the $\delta^{18}O$ value of precipitation was known. The nearest IAEA Isotopes in Precipitation collection stations to Cape Range are located at Darwin, Northern Territory (within the IASM regime) and at Perth, Western Australia (within the winter rainfall regime) (Fig. 1). Monthly average rainfall data from Perth reveal a precipitation $\delta^{18}O$/air temperature relationship of +0.2‰/°C and amount effects of approx. −1‰/100 mm/month, with winter rain $\delta^{18}O$ values ranging from −3.5‰ to −4.1‰ (IAEA/WMO). Monthly average summer monsoon rainfall $\delta^{18}O$ values obtained at Darwin average −6‰ and yield no statistically significant relationship with air temperature but do exhibit an amount effect of approx. −1‰/100 mm/month (IAEA/WMO) (Fig. 8). Combining the temperature signal in winter rainfall from Perth (+0.2‰/°C) with the temperature dependence of oxygen isotopic fractionation of calcite crystallization (−0.2‰/°C) (Kim and O'Neil, 1997) results in an essentially temperature-insensitive stalagmite paleothermometer, and temperature effects are further complicated by the contribution of moisture derived from tropical cyclones, the $\delta^{18}O$ values for which are dominated by amount effects rather than air temperature (Lawrence and Gedzelman, 1996).

Applying such isotopic measurements of precipitation from distal stations is a source of considerable uncertainty and modern rainfall $\delta^{18}O$ values at Cape Range are not well constrained. Dogramaci et al. (2012) report three years of precipitation and groundwater oxygen isotopic values for the Hamersley Basin, located approximately 400 km east of Cape Range. Precipitation $\delta^{18}O$ values were highly variable over this interval and appeared to reflect amount effects, with the heavy rainfall (>20 mm) events that dominate the area's groundwater recharge averaging −6.7 ± 5.5‰; shallow groundwater values were more tightly clustered at −8.0 ± 0.8‰. Liu et al. (2010) modeled Australian precipitation oxygen isotopic values based on latitude, longitude, and altitude, and applying their model to Cape Range produces an average rainfall oxygen isotopic value of −6.2‰, a result identical to water from the Cape Range groundwater estuary (salinity = 1.9 p.s.u.) sampled in September 2011. Using the calcite-water paleothermometer of Craig (1965), water with this composition, coupled with the average middle Holocene stalagmite $\delta^{18}O$ value of −8.0 ± 0.3‰, yields a calcite crystallization temperature of 25 ± 1 °C, identical to modern mean annual temperature of Cape Range and consistent with the middle Holocene temperature reconstruction of van der Kaars et al. (2006). Nonetheless, stalagmite-based paleo-temperature estimates are untenable for the deglacial and LGM given the

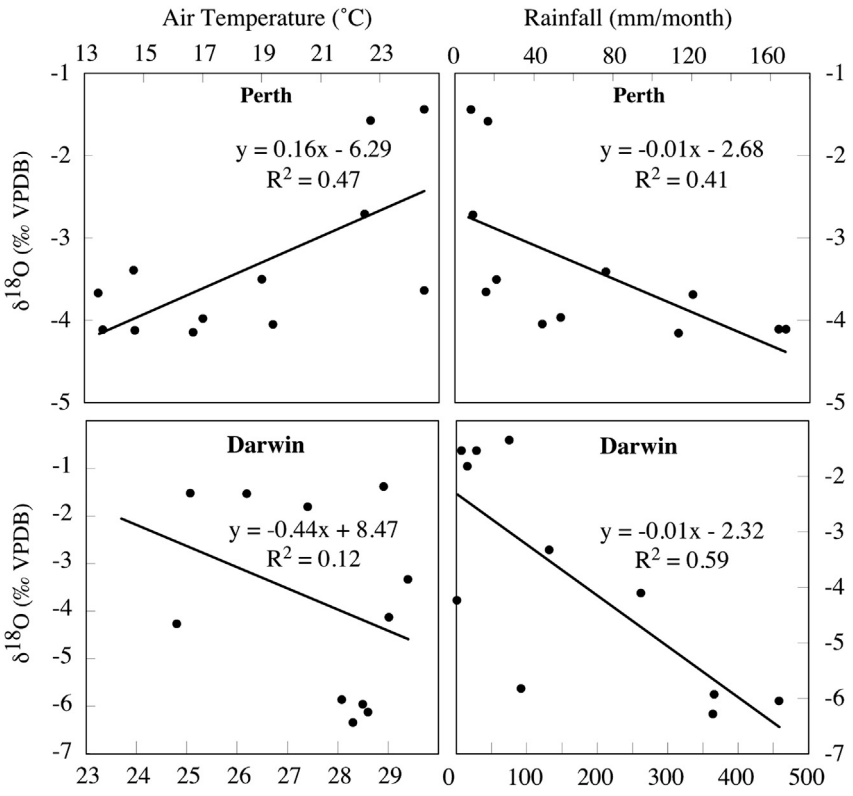


**Fig. 8.** Top – Oxygen isotopic ratios in rainwater relative to air temperature (Perth) and rainfall amount (Darwin).

possibility of changing contributions of moisture sources and their respective oxygen isotopic ratios on Cape Range precipitation $\delta^{18}O$ values. Substantial differences in $\delta^{18}O$ values between summer and winter precipitation is theoretically sufficient to allow stalagmites to track temporal changes in the relative influence of seasonal moisture, a technique similarly applied to studies of speleothems that grew during the Last Glacial cycle in the southwestern United States (Asmerom et al., 2010). However, our limited understanding of the evolution of these moisture sources under modern conditions, coupled with increased uncertainty regarding the positioning and strength of the IASM, southern westerlies, tropical cyclones, and northwest cloud bands during the late Pleistocene places the goal of *uniquely* constraining the roles of moisture source variations on C126 stalagmite oxygen isotopic variability beyond our ability.

### 5.3. *Influences of winter precipitation*

The deglacial C126 oxygen isotopic record is dominated by the negative oxygen isotopic anomaly coincident with Heinrich Stadial 1 (HS1), a feature that may be explained by changing contributions of winter rainfall. Variations in positioning of the southern hemisphere westerlies during the Last Glacial cycle have been suggested from geomorphic evidence across South America (Heusser, 1989), Africa (Mills et al., 2012), and Australia (Schulmeister et al., 2004) including a more northward position during glacial periods (Toggweiler et al., 2006; Fletcher and Moreno, 2012). Evidence for precipitation changes associated with migration of the southern hemisphere westerlies has also been obtained from south-central Australia, where megalake level markers track variations in hydrologic balances across the Last Glacial cycle (Cohen et al., 2011). Some of these interior basins, such as Lake Eyre, are located south of the area receiving monsoon rainfall, but contain vast catchment areas that reach far enough north to capture monsoon-derived runoff (Magee et al., 2004). Water levels in other nearby basins have been demonstrated to reflect contributions from southerly sources, as well. One such site, Lake Frome, experienced significant lake level fluctuations during the deglacial period, including lake level highs at 17.6–15.8 and 13.5–12.0 ka (Cohen et al., 2011) (Fig. 1; Fig. 7), and which have been tied to increased precipitation from southerly sources. This interpretation is supported by stalagmites from southern Australia (~30°S) that reveal accelerated growth from 17.1 to 15.8 ka (Cohen et al., 2011) and by an equatorward shift in polar waters at this time (Barrows and Juggins, 2005). However, using multi-proxy analysis of a marine core just south of the Australian margin, De Deckker et al. (2012) documented deglacial changes in the strength of the Leeuwin Current which, in turn, reflect positioning of the Subtropical Front and the southern hemisphere westerlies. These data reveal an anti-phasing with the North Atlantic such that *poleward* migration of the southern hemisphere westerlies occurred synchronously with HS1 and HS2, possibly due to linkages to AMOC, and thus rainfall from these sources should have been generally reduced across southern Australia during HS1. However, concentrations of Fe from aeolian dust within the same marine core record a sharp *drop* in South Australia continental aridity beginning at 17.5 ka. Taken together, these results may indicate that the relationship between positioning of the southern westerlies and rainfall balances across the southern portion of Australia were not necessarily straightforward. The C126 stalagmite record oxygen isotopic anomaly shows a structural similarity to this reconstruction of Leeuwin Current strength, although it is unclear whether there is a causal link between the two sites.

While some uncertainties therefore exist between the megalake and marine core records, it is clear that the southern hemisphere westerlies, along with associated storm tracks, are important

components of winter rainfall in southern Australia today, and thus latitudinal shifts of their position would have impacted southern and possibly also central Australia precipitation patterns. Reductions in South Australia aridity are coincident with periods of decreased $\delta^{18}O$ values in C126 stalagmites, and given the predominance of modern winter rainfall at Cape Range, equatorward migration of the westerlies may explain Last Glacial and early Holocene climate variability at C126. This interpretation is challenged, however, by precipitation reconstructions from pollen data obtained from the Cape Range margin and interpreted using transfer functions developed by van der Kaars et al. (2006). Although containing substantial short-term variability, when smoothed, these data suggest increases in summer rainfall and decreases in winter rainfall from the LGM to the early Holocene. In addition, HS2 is not apparent in the C126 record, although the relatively weak response of HS2 in the marine core taken south of Australia similarly may suggest that it was limited in magnitude in this region.

Treble et al. (2005) conducted daily precipitation isotopic analyses over a year-long interval from Cape Leeuwin Lighthouse (34.5°S), located approximately 200 km south of Perth, and while they found precipitation $\delta^{18}O$ values consistent with those from Perth (weighted average of −4.3‰), they also identified a negative correlation with rainfall amount, with the largest amounts of rainfall associated with the lowest $\delta^{18}O$ values; no statistically significant correlation between precipitation and air temperature was evident (although ultra-high-resolution $\delta^{18}O$ analysis of early twentieth century stalagmite calcite from this area suggests a breakdown in amount effects on precipitation at this time) (Treble et al., 2005). These $^{18}O$-depleted rainfall events were delivered by low pressure systems in the Southern Ocean that passed closest to the South Australian coast. These data suggest that moisture derived from southern sources such as these may have been more isotopically-depleted further north in association with equatorward migration of the southern hemisphere westerlies.

Next, given their prominent influence on modern moisture budgets at Cape Range today, changes in the strength or frequency of NWCB must also be considered. Observational and modeling studies demonstrate a correlation between northwest Australia rainfall and SST (and SST gradients; Shi et al., 2008) in the tropical eastern Indian Ocean (Fredericksen et al., 2011). Over the Last Glacial cycle, this region experienced marked changes in SST driven by changes in the strength of the Indonesian Throughflow (Zuraida et al., 2009). Oxygen isotopic and Mg/Ca analyses of foraminifera taken from a core located at the southwestern margin of the Timor Straight (13°5′S, 121°47′E), the main outflow for the Indonesia Throughflow, record SST variations that rose sharply during HS 3–5, with minimum SST of ~19.5 °C prior to HS and peak SST of 22–24 °C during HS. If similar SST changes coincided with HS1, then they could have driven a concomitant increased rainfall response across northwestern Australia.

Additional sources of eastern Indian Ocean SST variability, at least during the Holocene, have been the IOD and ENSO. Ashok et al. (2003) found a statistically significant reduction in western Australian winter rainfall during positive IOD years, although they did not investigate impacts on rainfall during negative IOD years. And Telcik (2003) noted an apparent inverse relationship between the IOD and NWCB activity. Abram et al. (2007) attributed SST variations in the northeastern Indian Ocean to strengthened and more frequent IOD activity during the middle Holocene relative to today which could have resulted in enhanced rainfall during negative IOD events. Regional SST in the NWCB-generating region are also influenced by ENSO with El Niño (La Niña) events resulting in less (more) warm surface water passing through the Indonesian Throughflow into the eastern Indian Ocean (Meyers, 1996), and resulting in diminished (enhanced) NWCB production (Wright, 1997; Telcik, 2003). However, changes in rainfall alone do not necessarily equate with changing precipitation (and therefore stalagmite) $\delta^{18}O$ values, and given the lack of isotopic data for precipitation associated with NWCB in northwest Australia, this mechanism remains largely untestable at the present time.

### 5.4. Influences of summer precipitation

The possibility also exists for a relationship between C126 stalagmite $\delta^{18}O$ variability and summer rainfall, which in the Cape Range region is largely attributable to tropical cyclone activity. Today, tropical cyclones contribute approximately 30% of the rainfall to the Cape Range (Milton, 1980; Dare et al., 2012; Indian Ocean Climate Initiative, 2012), and can deliver rainfall substantially lower in $\delta^{18}O$ values than average precipitation (Lawrence and Gedzelman, 1996; Lawrence, 1998; Lawrence et al., 2002). Lawrence and Gedzelman (1996) documented rainfall $\delta^{18}O$ values that ranged from −7 to −14‰ associated with Hurricane Gilbert (in contrast to non-cyclone-related summer rains which averaged −3‰) (IAEA/WMO) where it made landfall across Texas, USA in 1988 AD and tied these lightest values to isotopic exchange between inflowing vapor and falling rain. The area south of 18°S along the Western Australia coast is dominated by dry subsiding anticyclonic air masses associated with subtropical high pressure ridges. During the austral summer, moist air masses shift southeast, bringing with them convective thunderstorms, and in winter, rain may be derived from fronts that shift northward from the mid-latitudes. In general, the contribution of tropical cyclones to the annual hydrologic budget decreases with distance north and south of 18°S, in part because of the increase in rainfall derived from the IASM to the north and winter rainfall events to the south (Milton, 1980; Dare et al., 2012).

Tropical cyclone activity is linked to positioning of the ITCZ (Wang and Magnusdottir, 2006), and the coastal area just north of Cape Range is characterized by the highest average frequency of severe tropical cyclones in Western Australia (bom.gov.au) (Fig. 1). Therefore, southward migration of the ITCZ conceivably could have pushed this tropical cyclone activity further southward, resulting in elevated landfall events at Cape Range, and concomitant decreases in average annual precipitation $\delta^{18}O$ values. Prerequisites for tropical cyclone genesis include minimum SST of ~26.5 °C (Nicholls, 1979; Dare and McBride, 2011) and variations in SST associated with changes in Indonesian Throughflow form an additional, poorly constrained influence on cyclone activity as this would have impacted regional SST.

An alternative source of summer moisture during deglaciation may lie in the IASM. Recent IASM reconstructions from the southern Indo-Pacific Warm Pool (IPWP) (Flores and the Flores Sea; Fig. 1) reveal evidence for monsoon links to North Atlantic climate (Griffiths et al., 2009; Muller et al., 2012) with HS1 cooling in the North Atlantic Ocean forcing a southward displacement of the ITCZ through a reduction in Atlantic Meridional Overturning Circulation (AMOC) and increased ice cover in the high northern latitudes (Broccoli et al., 2006). Similar isotopic variability was documented in stalagmites from Ball Gown Cave in the western Kimberley region of tropical Australia and which also showed a close similarity to North Atlantic climate variations, with both HS1 and the Younger Dryas marked by periods of enhanced IASM moisture and the Bølling/Allerød characterized by a dramatic weakening in the IASM (Denniston et al., 2013) (Figs. 1 and 9). The similarity of the $\delta^{18}O$ record from C126 and the southern IPWP and western Kimberley suggests that this monsoon displacement was regional in scale, and thus raises the question of whether an increase in the contribution of C126 dripwater derived from isotopically light IASM sources was responsible for decreasing stalagmite $\delta^{18}O$ values during HS1.

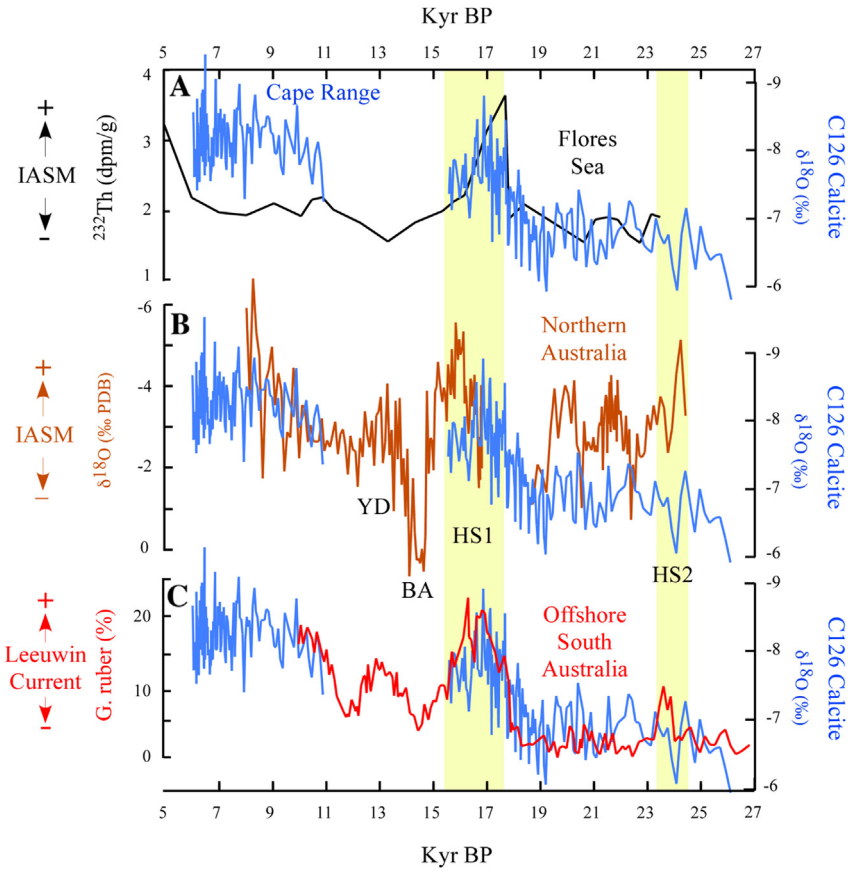


**Fig. 9.** Comparison of C126 oxygen isotopic time series (blue) with records of (A) IASM strength from Th abundances in Flores Sea core VM33-80 (Muller et al., 2012); (B) IASM strength from stalagmite oxygen isotopic ratios at Ball Gown Cave, tropical Western Australia (Denniston et al., 2013); (C) Leeuwin Current strength from *G. ruber* abundances in South Australia marine core MD03-2611 (De Deckker et al., 2012). Vertical yellow bars indicate Heinrich Stadials 1 (HS1) and 2 (HS2).

Interestingly, the C126 record does not preserve an isotopic anomaly coincident with HS2 (24.5–23.5 ka) (Fig. 9), but HS2 may have imparted a substantially smaller climatic response in the western Pacific than did HS1, an interpretation supported by the Chinese stalagmite record (Wang et al., 2001) as well as a South Australia marine core (De Deckker et al., 2012) and the Ball Gown Cave record (Denniston et al., 2013). Alternatively, the IASM may have been sufficiently weakened during the LGM such that southward migration of the ITCZ and the monsoon trough failed to deliver a sufficient increase in $^{18}$O-depleted moisture to Cape Range during HS2 so as noticeably decrease stalagmite $\delta^{18}$O values. In this scenario, in which close teleconnections exist between Western Australia and the North Atlantic, the gap in growth between the top of C126-118 and the bottom of C126-117 is perhaps related to northward migration of the IASM during Bølling/Allerød warming in the high northern latitudes, although changes in cave plumbing (infiltration pathways) are another possible source of the hiatus. Geomorphic evidence from the Fitzroy River and Lake Gregory, northwestern Australia, supports a significant strengthening of monsoon activity only around 14 ka (Wyrwoll and Miller, 2001) and pollen evidence from off-shore Cape Range supports increases in monsoon rainfall at 14 ka (van der Kaars and De Deckker, 2002; van der Kaars et al., 2006) (Fig. 1). Reconciling the hypothesis of a climatic origin for the missing stalagmite growth interval with the IASM data will therefore require further investigation.

The decrease in stalagmite $\delta^{18}$O values from 11 to 9 ka marks the earliest Holocene and is not coincident with a period of North Atlantic cooling but is instead characterized by rapid sea level rise that led to flooding of the Indo-Pacific continental shelves (Fig. 1). Early Holocene strengthening of the IASM has been linked to changing sea level (Griffiths et al., 2009), and thus at Cape Range, Holocene moisture balances may reflect an overall higher contribution of IASM rainfall than occurred during most of the LGM and the rest of the deglaciation. Similarly, the distribution of summer rainfall vs winter rainfall-related plant taxa in Lake Frome (Singh and Luly, 1991) and oxygen isotopic ratios from speleothems located proximally to Lake Frome (Quigley et al., 2010) argue for more southerly penetration of IASM moisture during the early/middle Holocene than occurs today.

### 5.5. Origins of carbon isotopic variability

Carbon isotopic ratios from C126 stalagmites offer a complementary view of climate dynamics at Cape Range. Like the oxygen isotopic time series, carbon isotopic ratios remained relatively heavy (~−5‰) from 26 to 19 ka, after which point they decreased by 7‰ to −12‰ between 8 and 5.5 ka (Fig. 7). The pronounced decrease in $\delta^{13}$C values is interpreted here to reflect enhanced biologic $CO_2$ production in soils overlying the cave due to increased temperature and rainfall in the early Holocene. The pollen transfer functions of van der Kaars et al. (2006) argue for a ~50% increase in mean rainfall over this time coupled with a rise in mean annual temperature of ~1 °C. Wetter conditions are generally associated with reduced PCP, and a warmer, wetter environment, coupled with higher atmospheric $CO_2$ concentrations (Schmitt et al., 2012), would have favored plant growth, thereby increasing soil

respiration and vegetation density (Hellstrom et al., 1998). Changes in the $C_3/C_4$ ratio of vegetation over the cave may have been responsible for the observed 7‰ decrease in carbon isotopic values from the LGM to the Holocene but the dominance of $C_4$ vegetation at Cape Range today necessitates that if plant type alone drove stalagmite $\delta^{13}C$ shifts from 20 to 7 ka, then an almost complete replacement by $C_4$ plants has occurred since the middle Holocene, a shift that is not recorded in regional pollen data (van der Kaars and De Deckker, 2002). Alternatively, the large decrease in stalagmite carbon isotopic values from 15 to 9 ka is a function of (or some combination of) elevated atmospheric $CO_2$ concentrations, temperatures, and precipitation that increased vegetation density and plant respiration, and thus the proportion of biogenic soil $CO_2$ relative to atmospheric $CO_2$ in the infiltrating fluids, and that may have also been associated with a decrease in PCP (Fig. 7).

The concomitant decreases in carbon and oxygen isotopic ratios from 19 to 17 ka may be explained by a similar mechanism. In this arid deglacial climate, plant density would have responded to increases in moisture, thereby elevating the production of soil $CO_2$, limiting the relative contribution of atmospheric $CO_2$ in infiltrating fluids, and thereby decreasing stalagmite $\delta^{13}C$ values. Although stalagmite growth rates reflect a myriad of influences, in arid climates, effective moisture exerts a first-order control (Asmerom and Polyak, 2004; Mattey et al., 2008). Therefore, the association of elevated growth rates in both C126-117 and C126-118 with the most negative $\delta^{13}C$ values likely reflects increased delivery of dripwater to the stalagmite surface during periods of greater plant density over the cave.

Under the current climate, deep caves such as C126 are seldom seen with active drips on the stalagmites. In the absence of modern calcite deposition, it remains unclear why middle Holocene stalagmite $\delta^{13}C$ values are characteristic of $C_3$-dominated vegetation over the cave site. One possibility is that vegetation has shifted dramatically since 6 ka in response to changing rainfall conditions. In fact, van der Kaars et al. (2006) document peak Holocene rainfall at 6 ka, followed by substantial decreases in both summer and annual average rainfall to the present, consistent with our data. The Lake Frome and associated stalagmite records preserve evidence of a middle Holocene ($\sim$5 ka) highstand which was tied to southward migration of the IASM trough and resulting tropical rainfall (Singh and Luly, 1991; Quigley et al., 2010; Cohen et al., 2011) rather than winter moisture, and if correct, then this monsoon influence would likely have been felt at Cape Range, as well. In addition, some effects may be related to PCP and/or kinetic-driven fractionation that decreased stalagmite $\delta^{13}C$ values through disequilibrium between the calcite and dissolved inorganic carbon reservoirs, an effect linked in tropical speleothems to negative shifts in stalagmite $\delta^{13}C$ values (Mickler et al., 2004).

## 6. Conclusions

Paleoenvironmental signals in stalagmites from Cape Range, Western Australia generally track glacial boundary conditions during the LGM and deglaciation. Origins of millennial-scale oxygen isotopic variability likely reflect multiple influences, including shifts in winter moisture related to positioning of the southern hemisphere westerlies, variations in IASM rainfall, and/or tropical cyclone activity. A shift to lower stalagmite calcite $\delta^{18}O$ values coincident with HS1 likely reflects changing moisture or moisture source that could involve the positioning of the southern hemisphere westerlies, an increase in the strength/and or location of the IASM trough, tropical cyclone activity, and/or northwest cloud band activity. In the absence of a clear relationship between air temperature and precipitation $\delta^{18}O$ values at Cape Range, it appears that temperature exerted at most a small influence on C126 stalagmite oxygen isotopic variability. Interestingly, the magnitude of the $\delta^{18}O$ anomaly coincident with HS1 is similar to the Pleistocene/Holocene oxygen isotopic shift, however no oxygen isotopic excursion is associated with HS2. Stalagmite $\delta^{13}C$ data indicate a dominant $C_4$ vegetation type during the drier and colder LGM period, with a transition to more prominent $C_3$ vegetation being complete by the middle Holocene (ca 5.5–7.0 ka), although the roles of PCP and kinetic fractionation on stalagmite carbon isotopic values cannot be ruled out. Decreased $\delta^{13}C$ values in the early Holocene are a response to increased effective moisture, temperature and possibly also atmospheric carbon dioxide levels. A middle Holocene minimum in stalagmite $\delta^{13}C$ and $\delta^{18}O$ values may reflect increased IASM rainfall, as recorded by regional pollen evidence.

## Acknowledgments

This work was funded by grants from the National Estates Grants Program (to WFH), the Center for Global and Regional Environmental Research and Cornell College (to RFD), and NSF EAR-0521196 (to MSL) and EAR-0326902 (to YA). We thank Darren Brooks for assistance in recovering the samples in 1991 under funding from the National Estate Program, a Commonwealth-financed grants scheme administered by the Australian Heritage Commission (Federal Government) and the Western Australian Heritage Committee (State Government). Sample collection and archiving information is available from WFH. This manuscript benefitted from discussions with Karl-Heinz Wyrwoll, Charitha Pattiaratchi, Ming Feng, Glenn Cook, and Bart Geerts, as well from comments by two anonymous reviewers.

## References

Abram, N.J., Gagan, M.K., Liu, Z., Hantoro, W.S., McCulloch, M.T., Suwargadi, W., 2007. Seasonal characteristics of the Indian Ocean Dipole during the Holocene epoch. Nature 445, 299–302.

Ashok, K., Guan, Z., Yamagata, T., 2003. Influence of the Indian Ocean Dipole on the Australian winter rainfall. Geophysical Research Letters 30, 1821. http://dx.doi.org/10.1029/2003GL017926.

Asmerom, Y., Polyak, V., 2004. Comment on Betancourt et al. (2002) "A test of annual resolution in stalagmites using tree rings." Quaternary Research 61, 119–121.

Asmerom, Y., Polyak, V., Burns, S., 2010. Variable winter moisture in the southwestern United States linked to rapid glacial climate shifts. Nature Geoscience 3, 114–117.

Baker, A., Ito, E., Smart, P.L., McEwan, R.F., 1997. Elevated and variable values of $^{13}C$ in speleothems in a British cave system. Chemical Geology 136, 263–270.

Barrows, T.T., Juggins, S., 2005. Sea-surface temperatures around the Australian margin and Indian Ocean during the last glacial maximum. Quaternary Science Reviews 24, 1017–1047.

Broccoli, J.E., Dahl, K.A., Stouffer, R.J., 2006. Response of the ITCZ to Northern Hemisphere cooling. Geophysical Research Letters 33, L01702.

Cerling, T.E., 1984. The stable isotopic composition of modern soil carbonate and its relationship to climate. Earth and Planetary Science Letters 71, 229–240.

Chen, J., Edwards, L., Wasserburg, W., 1986. $^{238}U$, $^{234}U$, and $^{232}Th$ in seawater. Earth and Planetary Science Letters 80, 241–251.

Cheng, H., Edwards, R.L., Hoff, J., Gallup, C.D., Richards, D.A., Asmerom, Y., 2000. The half-lives of U-234 and Th-230. Chemical Geology 169, 17–33.

Cohen, T.J., Nanson, G.C., Jansen, J.D., Jones, B.G., Jacobs, Z., Treble, P., Price, D.M., May, J.-H., Smith, A.M., Ayliffe, L.A., Hellstrom, J.C., 2011. Continental aridification and the vanishing of Australia's megalakes. Geology 39, 167–170.

Craig, H., 1965. The measurement of oxygen isotope paleotemperatures. In: Tongiorgi, E. (Ed.), Stable Isotopes in Oceanographic Studies and Paleotemperatures. Consiglio Nazionale della Richerche Laboratorio di Geologia Nucleare, Pisa, pp. 161–182.

Dansgaard, W., 1964. Stable isotopes in precipitation. Tellus 16, 436.

Dare, R.A., Davidson, N.E., McBride, J.L., 2012. Tropical cyclone contribution to rainfall over Australia. Monthly Weather Review 140, 3606–3619.

Dare, R.A., McBride, J.L., 2011. The threshold sea surface temperature condition for tropical cyclogenesis. Journal of Climate 24, 4570–4576.

Day, C.C., Henderson, G.M., 2011. Oxygen isotopes in calcite grown under cave-analogue conditions. Geochimica et Cosmochimica Acta 75, 3956–3972.

De Deckker, P., Moros, M., Perner, K., Jansen, E., 2012. Influence of the tropics and southern westerlies on glacial interhemispheric asymmetry. Nature Geoscience 5, 266–269.

Denniston, R.F., González, L.A., Asmerom, Y., Baker, R.G., Reagan, M.K., Bettis III, E.A., 1999. Evidence for increased cool season moisture during the middle Holocene. Geology 27, 815–818.
Denniston, R.F., DuPree, M., Asmerom, Y., Polyak, V., Dorale, J.A., Carpenter, S., 2007. Episodes of increased aridity in the Late Holocene recorded by stalagmites from Devils Icebox Cave, Central Missouri, USA. Quaternary Research 68, 45–52.
Denniston, R.F., Wyrwoll, K.-H., Asmerom, Y., Polyak, V.J., Humphreys, W., Cugley, J., Woods, D., Peota, J., Greaves, E., 2013. North Atlantic forcing of millennial-scale Australian monsoon variability during the Last Glacial. Quaternary Science Reviews 72, 159–168.
Dogramaci, S., Skrzypek, G., Dodson, W., Grierson, P.F., 2012. Stable isotope and hydrochemical evolution of groundwater in the semi-arid Hamersley Basin of subtropical northwest Australia. Journal of Hydrology 475, 281–293.
Dorale, J.A., Liu, Z., 2009. Limitations of Hendy Test criteria in judging the paleoclimatic suitability of speleothems and the need for replication. Journal of Cave and Karst Studies 71, 73–80.
Dorale, J.A., Gonzalez, L.A., Reagan, M.K., Pickett, D.A., Murrell, M.T., Baker, R.G., 1992. A high-resolution record of Holocene climate change in speleothem calcite from Cold Water Cave, northeast Iowa. Science 258, 1626–1630.
Fairchild, I.J., Smith, C.L., Baker, A., Fuller, L., Spotl, C., Mattey, D., McDermott, F., E.I.M.F., 2006. Modification and preservation of environmental signals in speleothems. Earth-Science Reviews 75, 105–153.
Fletcher, M.-S., Moreno, P.I., 2012. Vegetation, climate and fire regime changes in the Andean region of southern Chile (38°S) covaried with centennial-scale climate anomalies in the tropical Pacific over the last 1500 years. Quaternary Science Reviews 46, 46–56.
Forth, J.R., 1973. Exmouth Water Supply Western Australia. Western Australian Geological Survey Annual Report 1972, pp. 11–15.
Frederiksen, J.S., Fredericksen, C.S., Osbrough, S.L., Sisson, J.M., 2011. Changes in Southern Hemisphere rainfall, circulation and weather systems. In: 19th International Congress on Modelling and Simulation, Perth, Australia, 12–16 December 2011. http://mssanz.org.au/modsim2011.
Frumkin, A., Ford, D.C., Schwarcz, H.P., 2000. Paleoclimate and vegetation of the Last Glacial cycles in Jerusalem from a speleothem record. Global Biogeochemical Cycles 14, 863–870.
Gentilli, J., 1986. Climate. In: Jeans, D.N. (Ed.), Australia, a Geography, The Natural Environment, vol. 1. Sydney University Press, Sydney, Australia, pp. 14–48.
Genty, D., Blamart, D., Ouahdi, R., Gilmour, M., Baker, A., Jouzel, J., Van-Exter, S., 2003. Precise dating of Dansgaard-Oeschger climate oscillations in western Europe from stalagmite data. Nature 421, 833–837.
Griffiths, M.L., Drysdale, R.N., Gagan, M.K., Zhao, J.X., Ayliffe, L.K., Hellstrom, J.C., Hantoro, W.S., Frisia, S., Feng, Y.X., Cartwright, I., Pierre, E.S., Fischer, M.J., Suwargadi, B.W., 2009. Increasing Australian-Indonesian monsoon rainfall linked to early Holocene sea-level rise. Nature Geoscience 2, 636–639. http://dx.doi.org/10.1038/ngeo605.
Hamilton-Smith, E., Kiernan, K., Spate, A., 1998. Karst Management Considerations for the Cape Range Karst Province, Western Australia. A Report Prepared for the Department of Environmental Protection, Perth, Western Australia.
Hattersley, P.W., 1983. The distribution of $C_3$ and $C_4$ grasses in Australia in relation to climate. Oecologia 57, 113–128.
Hellstrom, J., McCulloch, M., Stone, J., 1998. A detailed 31,000-year record of climate and vegetation change, from the isotope geochemistry of two New Zealand speleothems. Quaternary Research 50, 167–178.
Hendy, C., 1971. The isotopic geochemistry of speleothems – I. The calculation of the effects of different modes of formation on the isotopic composition of speleothems and their applicability as palaeoclimatic indicators. Geochimica et Cosmochimica Acta 35, 801–824.
Heusser, C.J., 1989. Southern westerlies during the Last Glacial Maximum. Quaternary Research 31, 423–425.
Humphreys, W.F., 1991a. Survey of Caves in Cape Range, North West Cape Peninsula, Western Australia. Unpublished Report Prepared Under the National Estate Grants Program, a Commonwealth-finance Grants Scheme Administered by the Australian Heritage Commission (Federal Government) and the Heritage Council of Western Australia (State Government).
Humphreys, W.F., 1991b. Experimental re-establishment of pulse-driven populations in a terrestrial troglobite community. Journal of Animal Ecology 60, 609–623.
IAEA/WMO: Global Network of Isotopes in Precipitation, The GNIP Database. http://isohis.iaea.org.
Indian Ocean Climate Initiative, 2012. In: Bates, B., Frederiksen, C., Wormworth, J. (Eds.), Western Australia's Weather and Climate: a Synthesis of Indian Ocean Climate Initiative Stage 3 Research. CSIRO and BoM, Australia, p. 117.
Kim, S.-T., O'Neil, J.R., 1997. Equilibrium and nonequilibrium oxygen isotope effects in synthetic carbonates. Geochimica et Cosmochimica Acta 61, 3461–3475.
Kohler, P., Fischer, H., Schmitt, J., 2010. Atmospheric $\delta^{13}CO_2$ and its relation to $pCO_2$ and deep ocean $\delta^{13}C$ during the late Pleistocene. Paleoceanography 25, PA1213.
Lachniet, M.S., 2009. Climatic and environmental controls on speleothem oxygen isotope values. Quaternary Science Reviews 28, 412–432.
Lawrence, J.R., 1998. Isotopic spikes from tropical cyclones in surface waters: opportunities in hydrology and paleoclimatology. Chemical Geology 144, 153–160.
Lawrence, J.R., Gedzelman, D., 1996. Low stable isotope ratios of tropical cyclone rains. Geophysical Research Letters 23, 527–530.
Lawrence, J.R., Gedzelman, S.D., Gamache, J., Black, M., 2002. Stable isotope ratios: Hurricane Olivia. Stable isotope ratios of precipitation collected at 3 km elevation in Hurricane Olivia (1994). Journal of Atmospheric Chemistry 41, 67–82.
Liu, J., Fu, G., Song, X., Charles, S.P., Zhang, Y., Han, D., Wang, S., 2010. Stable isotopic compositions in Australian precipitation. Journal of Geophysical Research 115, D23307.
Magee, J.W., Miller, G.H., Spooner, N.A., Questiaux, D., 2004. Continuous 150 k.y. monsoon record from Lake Eyre, Australia. Insolation-forcing implications and unexpected Holocene failure. Geology 32, 885–888.
Mattey, D., Lowry, D., Duffet, J., Fisher, R., Hodge, E., Frisia, S., 2008. A 53 year seasonally resolved oxygen and carbon isotope record from a modern Gibraltar speleothem: reconstructed drip water and relationship to local precipitation. Earth and Planetary Science Letters 269, 80–95.
Meehl, G.A., 1993. A coupled air-sea mechanism in the tropical Indian Ocean and Pacific regions: role of the ocean. Journal of Climate 6, 31–41.
Meyers, G., 1996. Variations of Indonesian throughflow and El Niño/Southern Oscillation. Journal of Geophysical Research 101 (C5), 12,255–12,263.
Mickler, P.J., Banner, J.L., Stern, L., Asmerom, Y., Edwards, R.L., Ito, E., 2004. Stable isotope variations in modern tropical speleothems: evaluating applications to paleoenvironmental reconstructions. Geochimica et Cosmochimica Acta 68, 4381–4393.
Miller, G.H., Magee, J.W., Jull, A.J.T., 1997. Low-latitude glacial cooling in the Southern Hemisphere from amino-acid racemization in emu eggshells. Nature 385, 241–244.
Mills, S.C., Grab, S.W., Rea, B.R., Carr, S.J., Farrow, A., 2012. Shifting westerlies and precipitation patterns during the Late Pleistocene in southern Africa determined using glacier reconstruction and mass balance modeling. Quaternary Science Reviews 55, 149–159.
Milton, D., 1980. The contribution of tropical cyclones to the rainfall of tropical Western Australia. Singapore Journal of Tropical Geography 1, 46–54.
Muller, J., McManus, J.F., Oppo, D.W., Francois, R., 2012. Strengthening of the Northeast Monsoon over the Flores Sea, Indonesia, at the time of Heinrich event 1. Geology 40, 635–638.
Nicholls, N., 1979. A possible method for predicting seasonal tropical cyclone activity in the Australian region. Monthly Weather Review 107, 1221–1224.
Nicholls, N., 1992. Recent performance of a method for forecasting Australian seasonal tropical cyclone activity. Australian Meteorology Magazine 40, 105–110.
Pearce, A., Pattiaratchi, C., 1999. The Capes Current: a summer countercurrent flowing past Cape Leeuwin and Cape Naturaliste, Western Australia. Continental Shelf Research 19, 401–420.
Pittock, A.B., 1975. Climatic change and the pattern of variation in Australian rainfall. Search 1, 498–504.
Quigley, M.C., Horton, T., Hellstrom, J.C., Cupper, M.L., Sandiford, M., 2010. Holocene climate change in arid Australia from speleothem and alluvial records. The Holocene 20, 1,093–1,104.
Romanek, C.S., Grossman, E.L., Morse, J.W., 1992. Carbon isotopic fractionation in synthetic aragonite and calcite: effects of temperature and precipitation rate. Geochimica et Cosmochimica Acta 56, 419–430.
Russell, P.J., 2004. Geological and Geomorphic Features and Evolution of the Lake McLeod – Ningaloo – Cape Range – Exmouth Gulf Area, Western Australia. Report prepared for the Department on Conservation and Land Management, Perth, Western Australia.
Saltzman, M.R., Thomas, E. Carbon isotope stratigraphy. In: Gradstein, F., Ogg, J., Ogg, G., Schmitz, M. (Eds.), The Geologic Time Scale 2012, pp. 207–232. http://dx.doi.org/10.1016/B978-0-444-59425-9.00011-1.
Schmitt, J., Schneider, R., Elsig, J., Leuenberger, D., Lourantou, A., Chappellaz, J., Köhler, P., Joos, F., Stocker, T.F., Leuenberger, M., Fischer, H., 2012. Carbon isotope constraints on the deglacial $CO_2$ rise from ice cores. Science 336, 711–714.
Schulmeister, J., Goodwin, I., Renwick, J., Harle, K., Armand, L., McGlone, M.S., Cook, E., Dodson, J., Hesse, P.P., Mayewski, P., Curran, M., 2004. The Southern Hemisphere westerlies in the Australasian sector over the Last Glacial cycle: a synthesis. Quaternary International 118–119, 23–53.
Shi, G., Cai, W., Cowan, T., Ribbe, J., Rotstayn, L., Dix, M., 2008. Variability and trend of North West Australia rainfall: observations and coupled climate modeling. Journal of Climate 21, 2938–2959.
Singh, G., Luly, J., 1991. Changes in vegetation and seasonal climates since the last full glacial at Lake Frome, South Australia. Palaeogeography, Palaeoclimatology, Palaeoecology 84, 75–86.
Smith, B.N., Epstein, S., 1971. Two categories of $C_3/C_4$ ratios for higher plants. Plant Physiology 47, 380–384.
Telcik, N., 2003. Influence of the Eastern Indian Ocean Variability on Southwest Australian Rainfall (Unpublished masters thesis). University of Western Australia, p. 159.
Toggweiler, J.R., Russel, J., Carson, S.R., 2006. Midlatitude westerlies, atmospheric $CO_2$, and climate change during the ice ages. Paleoceanography 21, PA2005.
Treble, P.C., Chappell, J., Gagan, M.K., McKeegan, K.D., Harrison, T.M., 2005. In situ measurement of seasonal $\delta^{18}O$ variations and analysis of isotopic trends in a modern speleothem from southwest Australia. Earth and Planetary Science Letters 233, 17–32.
van der Kaars, S., De Deckker, P., 2002. A Late Quaternary pollen record from deep-sea core Fr10/95, GC17 offshore Cape Range Peninsula, northwestern Western Australia. Review of Palaeobotany and Palynology 120, 17–39.
van der Kaars, S., De Deckker, P., 2003. Pollen distribution in marine surface sediments offshore Western Australia. Review of Palaeobotany and Palynology 124, 113–129.

van der Kaars, S., De Deckker, P., Gingele, F.X., 2006. A 100 000-year record of annual and seasonal rainfall and temperature for northwestern Australia based on a pollen record obtained offshore. Journal of Quaternary Science 21, 879–889.

Wang, Y.J., Cheng, H., Edwards, R.L., An, Z.S., Wu, J.Y., Shen, C.C., Dorale, J.A., 2001. A high-resolution absolute-dated late Pleistocene monsoon record from Hulu Cave, China. Science 294, 2345–2348. http://dx.doi.org/10.1126/science.1064618.

Wang, C.-C., Magnusdottir, G., 2006. The ITCZ in the central and eastern Pacific on synoptic time scales. Monthly Weather Review 134, 1405–1421.

WAPC, Western Australia Planning Commission, 1996. Environmental Protection of Cape Range Province; Position Statement 1. Environmental Protection Authority, ISBN 0 7309 8169 X, p. 28.

Wright, W.J., 1997. Tropical-extratropical cloudbands and Australian rainfall. I: Climatology. International Journal of Climatology 17, 807–829.

Wyrwoll, K.-H., Miller, G.H., 2001. Initiation of the Australian summer monsoon 14,000 years ago. Quaternary International 83-85, 119–128.

Zuraida, R., Holbourn, A., Nurnberg, D., Kuhnt, W., Durkop, A., Erichsen, A., 2009. Evidence for Indonesian throughflow slowdown during Heinrich events 3–5. Paleoceanography 24, PA2205.